

CIC-14 REPORT COLLECTION
**REPRODUCTION
COPY**

LALP-95-012-110

**CNLS
NEWSLETTER**

c. 3

Center for Nonlinear Studies
Los Alamos National Lab.
Los Alamos, NM 87545

No. 110, February 1995

CNLS SCIENCE ACTIVITY

**An  Experimental Investigation of Shock-Accelerated
Heavy Gas Layers**

John M. Budzinski^{1,2} and Robert F. Benjamin²

¹Center for Nonlinear Studies

²Dynamic Experimentation Division

Los Alamos National Laboratory

and

Jeffrey W. Jacobs

Dept. of Aerospace and Mechanical Engineering

Univ. of Arizona

ABSTRACT

Layers of a heavy gas surrounded by a lighter gas are accelerated by a Mach 1.2 shock. In the experiments, SF₆ is used as the heavy gas and air is the lighter gas. A corrugated nozzle creates a layer with perturbations on the upstream and downstream interfaces. For each experiment, the initial perturbation amplitude on one side of the layer can either be larger, smaller, or the same as the amplitude on the other side. These differences lead to the formation of the different post shock flow patterns. Planar laser Rayleigh scattering is used to study these patterns and correlate them with the initial condition. The formation of the different patterns is explained in terms of the Richtmyer-Meshkov instability of the sides of the layer, and in terms of vortex dynamics.

Introduction

Experiments are performed to study the different flow patterns created by shock accelerating a heavy gas layer. A planar laser Rayleigh scattering technique is used to view two-dimensional cross-sections of a laminar gas jet. To create the jet, we flow SF_6 through a corrugated nozzle, forming a varicose cross section, heavy gas layer. The flow is slightly unstable and the exact perturbations on the upstream and downstream interfaces changes randomly from experiment to experiment. This shock-layer interaction models many important flows found in engineering and science. As an example, this phenomenon may occur in inertial confinement fusion targets when the ablatively-driven impulse causes implosion of a fuel-containing shell. A potential difficulty is the mixing of shell material with the fuel, as a consequence of interfacial fluid instability.

When interfaces between different fluids are accelerated, they often become unstable, and any perturbations on the interface will grow. Rayleigh-Taylor instability occurs when a light fluid is accelerated into a heavy one, and the acceleration is constant. With this instability perturbations on the interface grow exponentially. However, if the heavy fluid is accelerated into the light, perturbations do not grow and the interface is stable. Richtmyer-Meshkov^{1,2} Instability (also known as the shock induced Rayleigh Taylor Instability) occurs when an interface between two fluids is accelerated impulsively. Here, the interface is unstable, regardless of the direction of the shock acceleration. However, if the shock moves from the light to heavy fluid, perturbations grow without a phase change, while if the shock moves from heavy to light, the perturbations on the interface will reverse phase and then grow. At later times the growth rate decreases, and mushroom shapes form from the peaks in the distorting interface.

Here, we continue our study³⁻⁵ of a shock interaction with a layer of heavy gas bounded on both sides by a lighter gas, where both interfaces of the layer have nearly sinusoidal perturbations. Thus each interface between fluids of different density involves the Richtmyer-Meshkov (RM) instability.

The results of a one-dimensional calculation of a shock interaction with an SF_6 layer are shown in Figure 1. Only the center of the expansion and compression waves are shown. Each time a wave interacts with an interface a transmitted and reflected wave are created. For a Mach 1.2 incident shock, the shock inside the layer is Mach 1.3, and the transmitted shock through entire layer is Mach 1.17. The wave reflected off the second interface leads to a series of waves inside the layer. Although the waves reverberate inside the layer, they are alternately compression and expansion waves so that the layer is always accelerated in the same direction. Each successive acceleration contributes to the interfacial instability on the sides of the layer. However, each wave is successively weaker, and the influence of these waves quickly become negligible.

The current experimental program was started by Jacobs *et al.*^{3,4}. They observed that three distinct flow patterns evolve from similar initial conditions, and speculated that differences in initial conditions might influence which flow pattern occurs during each event. These experiments observed only the dynamic flow condition for each event at one preset time because of limitations that precluded multiple image acquisition. We now report experiments where both initial and dynamic flow conditions are recorded for each event. The same three flows are observed, and have a strong correlation with asymmetries in the initial cross-section profile.

Experimental Apparatus

The present experiments employ improved optical techniques to capture two frames per event, shown schematically in Figure 2, but use the same shock tube and test section as in the earlier work.^{3,4} Our images are produced by the planar laser Rayleigh scattering (PLRS) of a laser sheet from the air and SF₆ gas molecules.^{5,6} Since the initial condition changes in an uncontrolled manner from experiment to experiment, we produced two images using two pulsed dye lasers, which illuminate the test region with coplanar sheets of laser light. Thus the exact initial condition and a dynamic image are viewed for each experiment. The images are recorded on a single, cooled CCD camera having 512 x 512 pixels. In contrast, the earlier experiments used fluorescent light produced by a tracer gas (diacetyl) injected into the SF₆ test gas. Thus, the present technique assures that we observe the flow of the test gases without reference to tracers, and enables direct measurement of the SF₆ concentration profile. Both the PLRS and PLIF methods are effective at overcoming problems of obscuration by wall effects associated with traditional schlieren and shadowgraphy methods.

The dye lasers operate at different wavelengths to enable spectral discrimination between the images of initial and dynamic flow conditions. The initial condition of the gas curtain is photographed just before shock impact using a laser having characteristics, 590 nm wavelength, about 10 μs duration and 1 J energy; the image is spectrally filtered through a Schott OG 515 longpass glass filter. The second image, showing the dynamic flow pattern, is produced with illumination from a laser at 480 nm, 0.5 μs and 0.4 J, filtered through an interference short pass filter. Our observation times of the dynamic condition were experimentally limited to between 100-500 μsec after the shock interaction. The Rayleigh scattering is weak, requiring great care to eliminate stray light. Because SF₆ scatters about six times more light than air, we observe good contrast between the regions of air and SF₆, and easy visualization of their interfaces. We convert the images to maps of SF₆ concentration by calibrating the system with scattering from pure air and pure SF₆.

The nozzle above the test section produces the laminar gas jet (i.e., the gas curtain) with a diffuse varicose cross section having a wavelength of about 6 mm and a peak to peak amplitude of

up to 2 mm on each side. The shock tube is fired when the gas curtain appears to be stable as observed with a real time schlieren system. With the improved diagnostic we can now measure the peak SF_6 concentrations in the layer, and find that the thicker regions of the layer contain about 50% SF_6 and the thinner regions about 40% SF_6 .

Results

Typical data from the experiments is shown in Figure 3. We observe the same three patterns after a Mach 1.2 shock interaction as seen in the earlier work, and find that asymmetries in the initial condition correlate with the three post-shock flow patterns in over 90% of the 100+ experiments performed. The post-shock flow pattern was classified visually as one of the three flow patterns based on the asymmetries present in the spacing of the pattern lobes and the SF_6 mass distribution, using the criteria described in Figure 4. The precise periodicity shown in the patterns in Figure 4 was usually not present in the data; irregularities often occurred as shown in the typical data, Figure 3. Mostly we find that an upstream mushroom pattern develops when the perturbations on the upstream side (i.e., on the side first interacting with the shock wave) are larger than the perturbations on the downstream side. A sinuous pattern forms when the perturbations on the downstream side are about the same or slightly larger than upstream side. A downstream mushroom develops when the perturbation on the downstream side is much larger than the perturbation on the upstream side. About 8% of the experimental images were anomalous and did not follow the correlation described above.

To quantify these dependencies, the amplitudes on the upstream and downstream interfaces were measured by finding the contours representing 50% of the layers maximum SF_6 concentration. Sample contours are shown in Figure 5a, in which the average position for each contour has been subtracted. The fourier coefficients for these contours are displayed in Figure 5b; the peaks corresponding to the imposed perturbation are at $n=4$, where n is the wave number. The amplitude for the upstream and downstream amplitudes were defined to be these peaks.

The contours and fourier coefficients were found for each experiment. Figure 6 shows the upstream amplitude vs. downstream amplitude for the experiments. Different symbols are used to distinguish between the different patterns observed. This plot confirms that upstream mushrooms form when the upstream amplitude is larger, downstream mushrooms form when the downstream amplitude is much larger, and the sinuous pattern forms between these regions. The plot shows the distribution is not symmetric. The boundary between the upstream and sinuous patterns occurs at a slope of about 1.2, while the boundary between the sinuous and downstream mushrooms occurs at a slope of about 0.3. Thus the angle covering the region of upstream mushrooms is significantly larger than the angle covering downstream mushrooms. This indicates a preference for generating upstream mushrooms over downstream mushrooms.

We speculate that there are at least two contributing factors for this preference. First, the upstream interface interacts with the shock and starts to grow before the downstream interface is shock accelerated. Thus the upstream interface has a head start, which must be overcome for a downstream to form. Second, for downstream mushrooms to occur, the heavy SF_6 must be accelerated faster than the surrounding air. Thus downstream mushrooms must fight the inertia of the heavy gas.

When the initial conditions fell near the lines separating the standard patterns, typically the post-shock pattern had characteristics of more than one pattern. For example, if the initial conditions had a downstream perturbation that was not large enough to produce a full downstream mushroom, and yet not small enough to produce a pure sinuous pattern, then by 0.45 msec after the shock interaction, well defined stems and caps would not be present, but the pattern would have some characteristics of the early-time downstream mushroom pattern.

We also find that the upstream mushrooms are aligned with the thicker parts of the initial layer whereas the downstream mushrooms are aligned with the thinner regions. Thus in the early development of downstream mushrooms, the heavy fluid moves laterally (i.e., normal to the shock direction) from the thicker to the thinner regions; there is less lateral movement of the heavy fluid during the early development of upstream mushrooms. When a sinuous pattern forms the downstream lobes are aligned with the thin regions of the initial layer and the upstream lobes are aligned with the thicker regions. We do not observe patterns with both upstream and downstream mushrooms.

Discussion

The observed nonlinear flow patterns can be interpreted qualitatively as the independent RM-instability growth of each interface, followed by strong coupling in the nonlinear growth regime. Richtmyer's impulse model¹ reasonably predicts the early-time growth rate of a single interface (shown recently in analyses^{7,8}). For our layer, the coupling between interfaces is initially weak⁷ when perturbation amplitudes are small, so the growth of each interface occurs independently. The impulse model predicts that the ratio of growth rates of the interfaces is equal to the ratio of initial perturbation amplitudes because the wavelengths, density ratios and final velocities are equal. Consequently, the interface with the larger amplitude will initially grow faster. This interface apparently dominates the nonlinear flow, as manifest by mushroom formation on the side with initially larger perturbation. Supporting this view is the observation that upstream mushroom caps are aligned with initially thicker regions of SF_6 , and downstream mushroom caps are aligned with thinner regions, as expected from the phase reversal property of RM instability. It is worth noting that if the interfaces remained weakly coupled in the nonlinear growth stage, one would expect to see post-shock flow patterns with both upstream and

downstream mushrooms in each experiment. Because these patterns are not observed, it appears that strong interface coupling in the nonlinear growth stage inhibits the formation of mushrooms on the side with initially smaller amplitude.

A complementary explanation for the observed flow patterns is based on viewing the flow evolution from the context of vortex dynamics. The vorticity (ω) is generated baroclinically by the shock interaction through the misalignment of pressure (P) and density (ρ) gradients:

$$\frac{D}{Dt}(\omega/\rho) = \frac{1}{\rho^3} \nabla \rho \times \nabla P + \text{non-baroclinic terms}$$

The dynamics of this vorticity then generates the growth of the layer. The magnitude of vorticity will be greatest where the pressure and density gradients are most misaligned. Assuming the pressure gradients are predominantly from planar waves, most of the vorticity is expected to be in the regions between the peaks and valleys of initial perturbations.

The different post-shock flows can be understood qualitatively by considering the differences in the vorticity production and transport during and immediately following shock acceleration. When the perturbation amplitude is greater on one side of the layer, more vorticity is generated on that side. Furthermore, the vorticity is preferentially generated in the lighter fluid, as seen by the density weighting in the vorticity equation. This effect accentuates the offset of the vorticity from the center of the layer. These effects are approximated in Figure 4 by representing the post-shock vorticity field by a row of vortices of alternating sign and offset from the center of the layer. The offset is shown exaggerated to emphasize the point. The mushrooms form on the side with the largest initial perturbation amplitude because the heavy fluid is asymmetrically entrained into the side with the most vorticity. The vorticity distribution of a symmetrically perturbed initial layer would be centered on the heavy layer and thus produce a sinuous pattern.

Conclusions

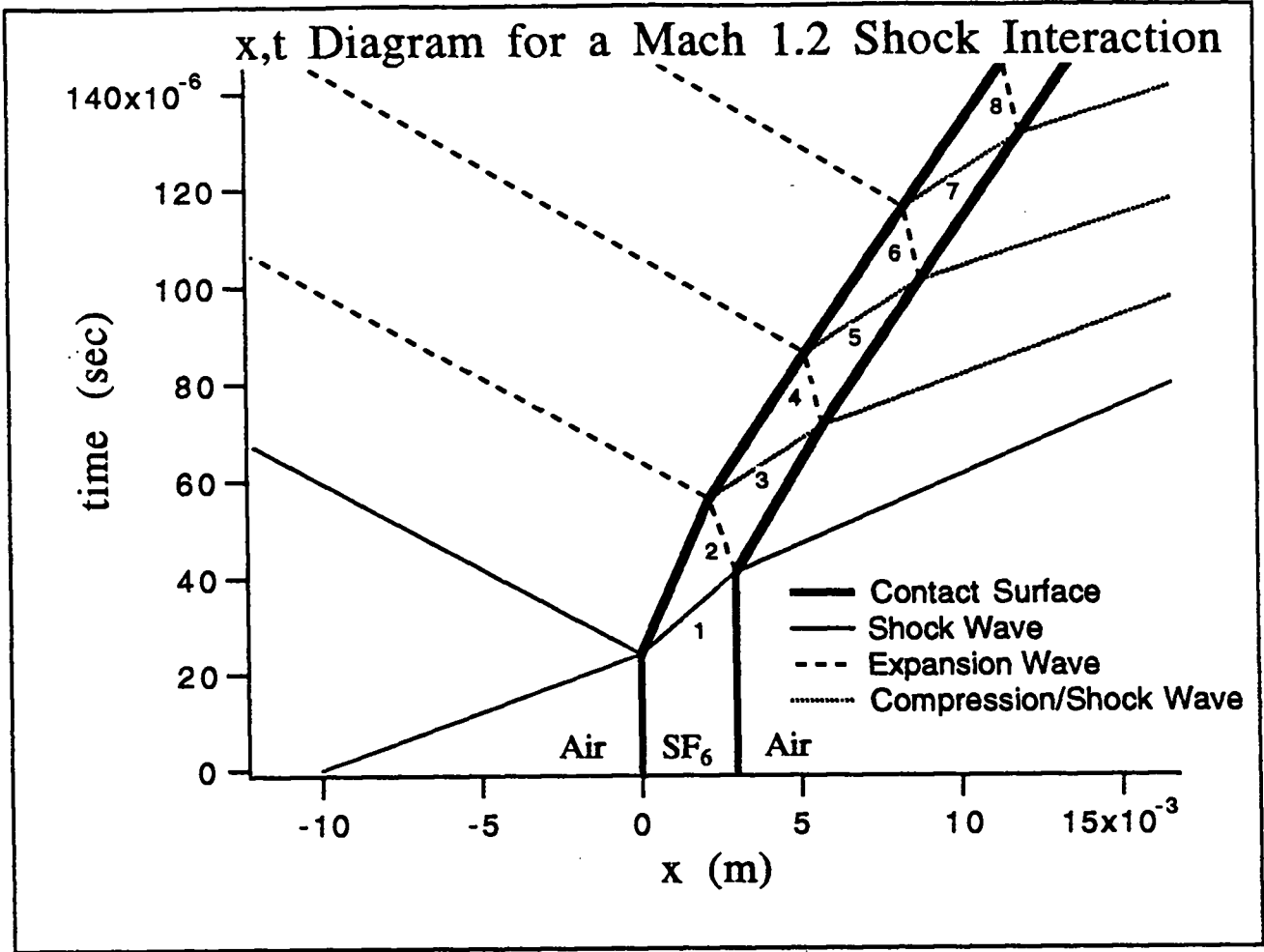
The patterns formed by shock accelerating a heavy gas layer can be understood by two complementary viewpoints. These viewpoints are based on the Richtmyer-Meshkov instability at each interface, and the baroclinic generation of vorticity followed by vortex dynamics domination of the flow evolution. Experimentally, multiple framing enables the correlation of initial perturbations with the appearance of each of the three distinct flow patterns induced by the shock-acceleration. We find that the ratio between the upstream and downstream perturbation amplitudes strongly influences which pattern forms. When this ratio is greater than about 1.2 upstream mushroom patterns usually develop. When the ratio is greater than 0.3 and less than 1.2, mostly sinuous patterns form. Finally when the amplitude ratio is less than 0.3 downstream mushrooms almost always form.

Acknowledgments

We acknowledge the continued encouragement of Harold Rogers and Harry Watanabe. We are also grateful for the suggestions of Rose Mary Baltrusaitis, David Sharp, and John Grove. We would like to thank Bob Critchfield for his technical support. The work was performed under the auspices of US Dept. of Energy, contract W-7405-ENG-36.

References

1. R. D. Richtmyer, "Taylor instability in shock acceleration of compressible fluids," *Commun. Pure Appl. Math.* **13**, 297-319(1960).
2. E. E. Meshkov, "Instability of the interface of two gases accelerated by a shock wave," *Izv. Akad. Nauk. SSSR Mekh. Zhidk. Gaza* **4**, 151-157 (1969) [*Fluid Dyn.* **4**, 101-104 (1969)].
3. J. W. Jacobs, D. L. Klein, D. G. Jenkins, and R. F. Benjamin, "Instability growth patterns of a shock-accelerated thin fluid layer," *Phys. Rev. Lett.* **70**, 583-586 (1993).
4. J. W. Jacobs, D. G. Jenkins, D. L. Klein, and R. F. Benjamin, "Nonlinear growth of shock-accelerated instability in a thin fluid layer," submitted to *Journal of Fluid Mechanics* (1993).
5. J. M. Budzinski, "Influence of initial conditions on the flow patterns of a shock-accelerated thin fluid layer." *Physics of Fluids* **6**, 3510-3512 (1992).
6. J. M. Budzinski, "Planar Rayleigh Scattering Measurements of Shock Enhanced Mixing," Ph.D. thesis at California Institute of Technology, 1992.
7. K. O. Mikaelian, "Growth rate of Richtmyer-Meshkov instability at shocked interfaces," *Phys. Rev. Lett.* **71**, 2903 (1993).
8. J. W. Grove, R. Holmes, D. H. Sharp, Y. Yang, Q. Zhang, "Quantitative theory of Richtmyer-Meshkov instability," *Phys. Rev. Lett.* **71**, 3473 (1993).



Wave Strengths	
wave	$\Delta P/P$
1	0.73
2	-0.167
3	0.066
4	-0.022
5	0.008
6	-0.002

Figure 1. x-t diagram for a Mach 1.2 shock interaction with a layer of heavy gas. Every time a wave interacts with an interface, a transmitted and reflected wave are created. This leads to a series of successively weaker waves which reverberate inside the layer. The reverberating waves alternate between expansion and compression waves, and consistently accelerate the layer to the right.

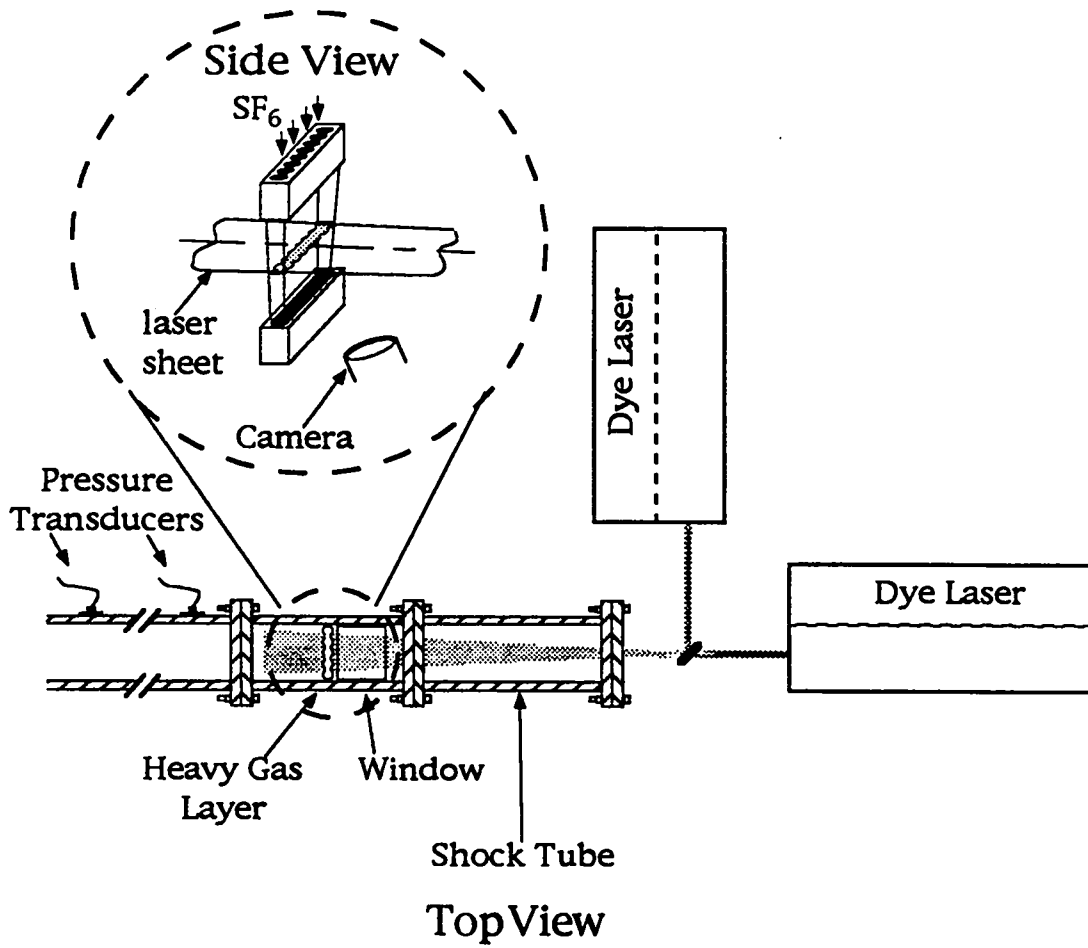


Figure 2. Experimental System. Two pictures, an initial condition and a post-shock dynamic image, are taken per experiment using planar laser Rayleigh scattering.

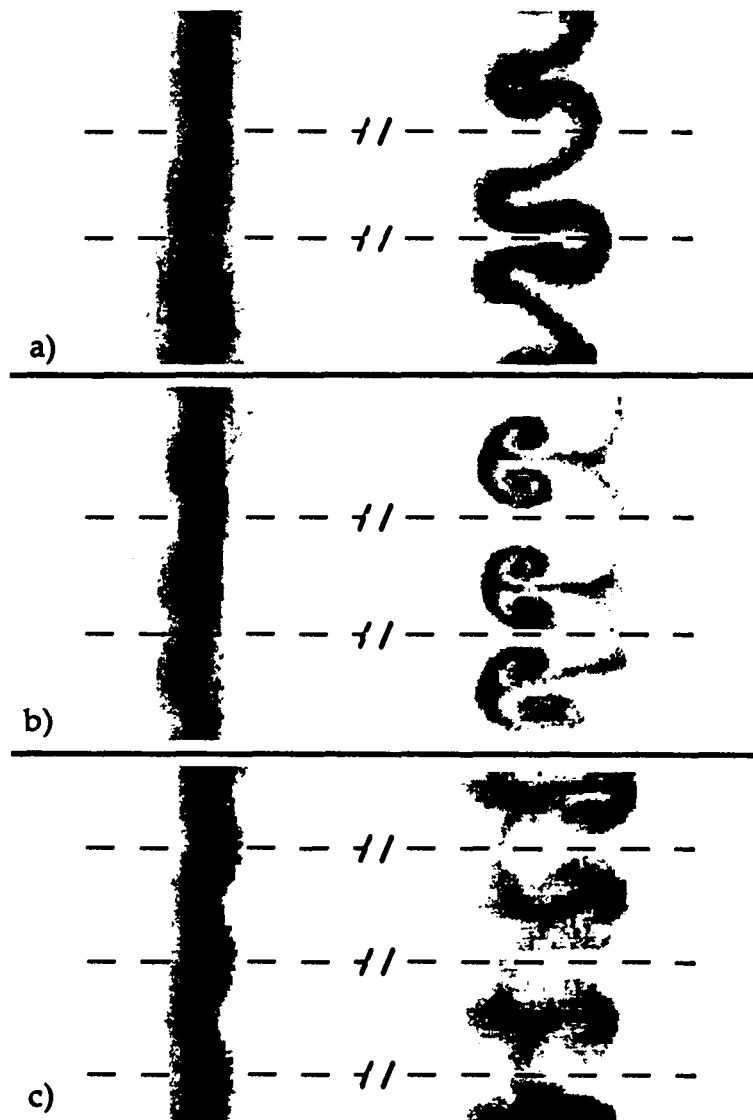


Figure 3. Composite of images from three typical experiments showing the initial and dynamic condition on each experiment. The shock wave moves left to right. The distance shown in the figure between the initial and dynamic condition of each pair is considerably less than the actual distance in the experiment. (a) $450 \mu\text{s}$ after a shock interaction. A sinuous pattern forms when the perturbation amplitude on the downstream side of the layer is about the same or slightly larger than the perturbation on the upstream and side. (b) $450 \mu\text{s}$ after a shock interaction. An upstream mushroom forms when the perturbation is larger on the upstream side of the layer. (c) $400 \mu\text{s}$ after a shock interaction. A downstream mushroom forms when the perturbation on the downstream side is significantly larger than the upstream side.

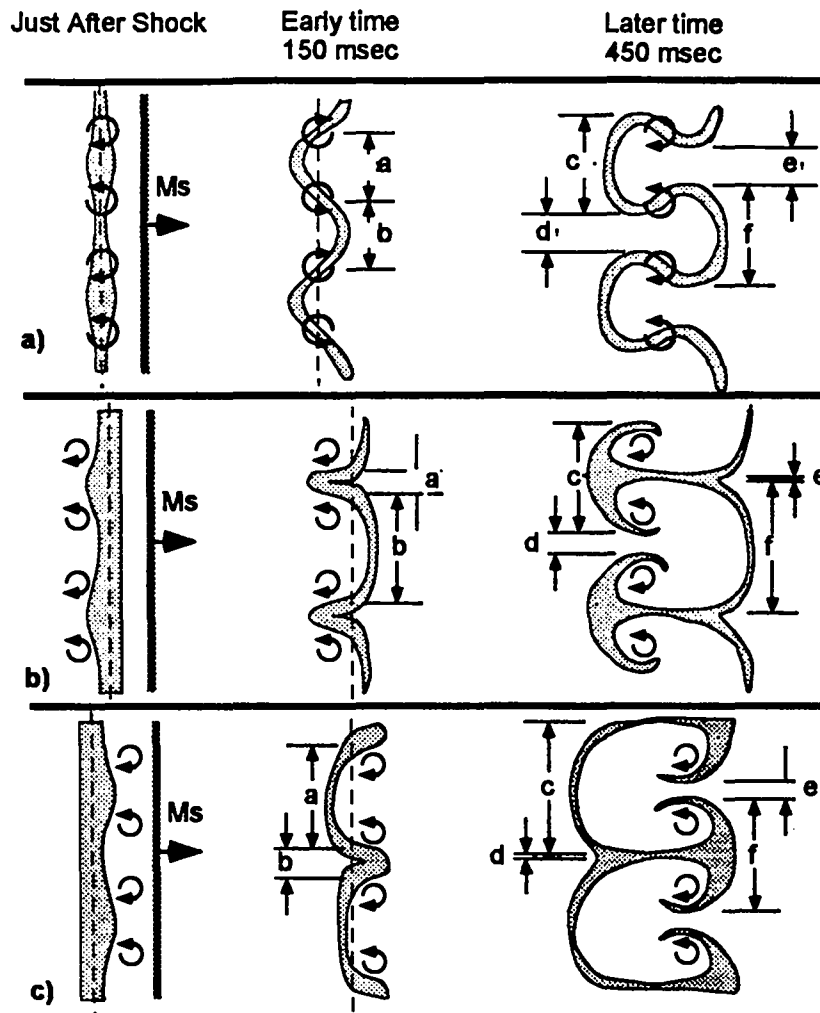
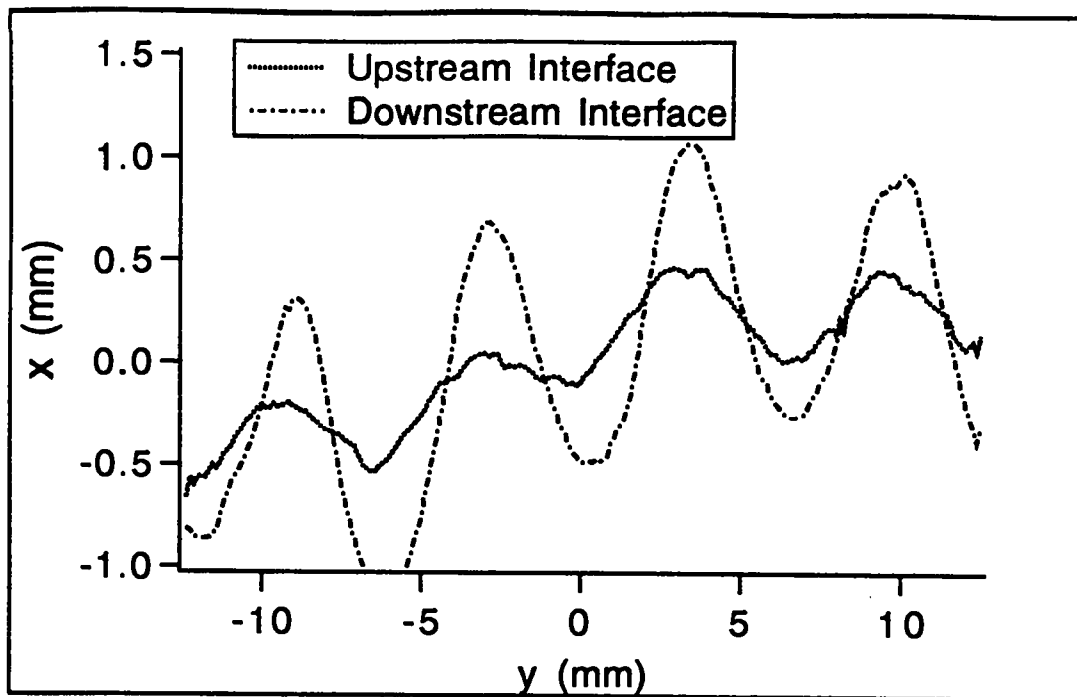
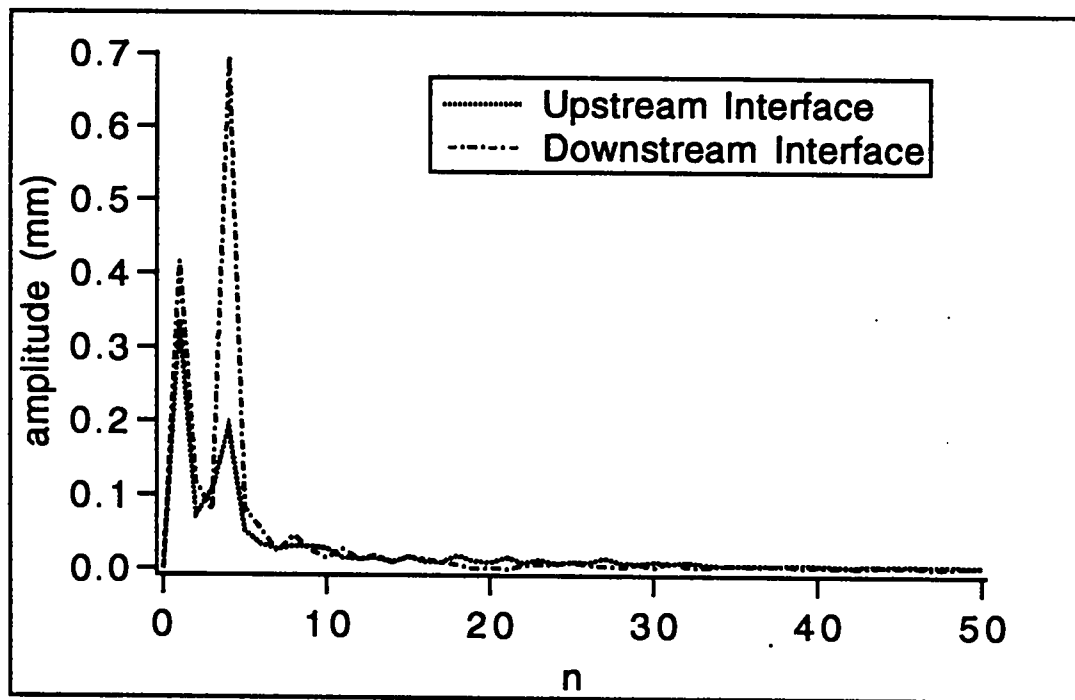


Figure 4. Differences in the different patterns throughout their development and a simple model to explain why they might occur. a) Sinuous pattern: perturbations are about equal on both sides of the layer, at early times $a \sim b$, at latter times $c \sim e$, $d \sim f$, and the SF_6 is evenly distributed throughout the layer. Just after the shock interaction the center of vorticity (shown by the circular arrows) is roughly in the center of the layer inducing the sinuous pattern to develop. b) Upstream mushroom pattern: The initial upstream perturbation amplitude is larger than the downstream, at early times $b > a$, at later times $d > e$, $c < f$. The highest SF_6 concentrations and most of the SF_6 mass is in the mushroom caps. Just after the shock interaction most of the vorticity is to the left of the layer. As the vorticity entrains the fluid the mushrooms form. c) Downstream mushroom pattern: The initial downstream perturbation amplitude is larger than the upstream. At early times $a > b$, at later times $d < e$, $c > f$. The highest SF_6 concentrations and most of the SF_6 mass is in the mushroom caps. Just after the shock interaction most of the vorticity is to the right of the layer. As the vorticity entrains the fluid, the mushrooms form.



(a)



(b)

Figure 5. Upstream and downstream interfaces of a typical initial condition. The initial condition is based on contours representing 50% of the maximum layer SF_6 concentration. (a) The contours with the mean position of each subtracted. (b) the fourier coefficients of the contours in a. n is the wave number.

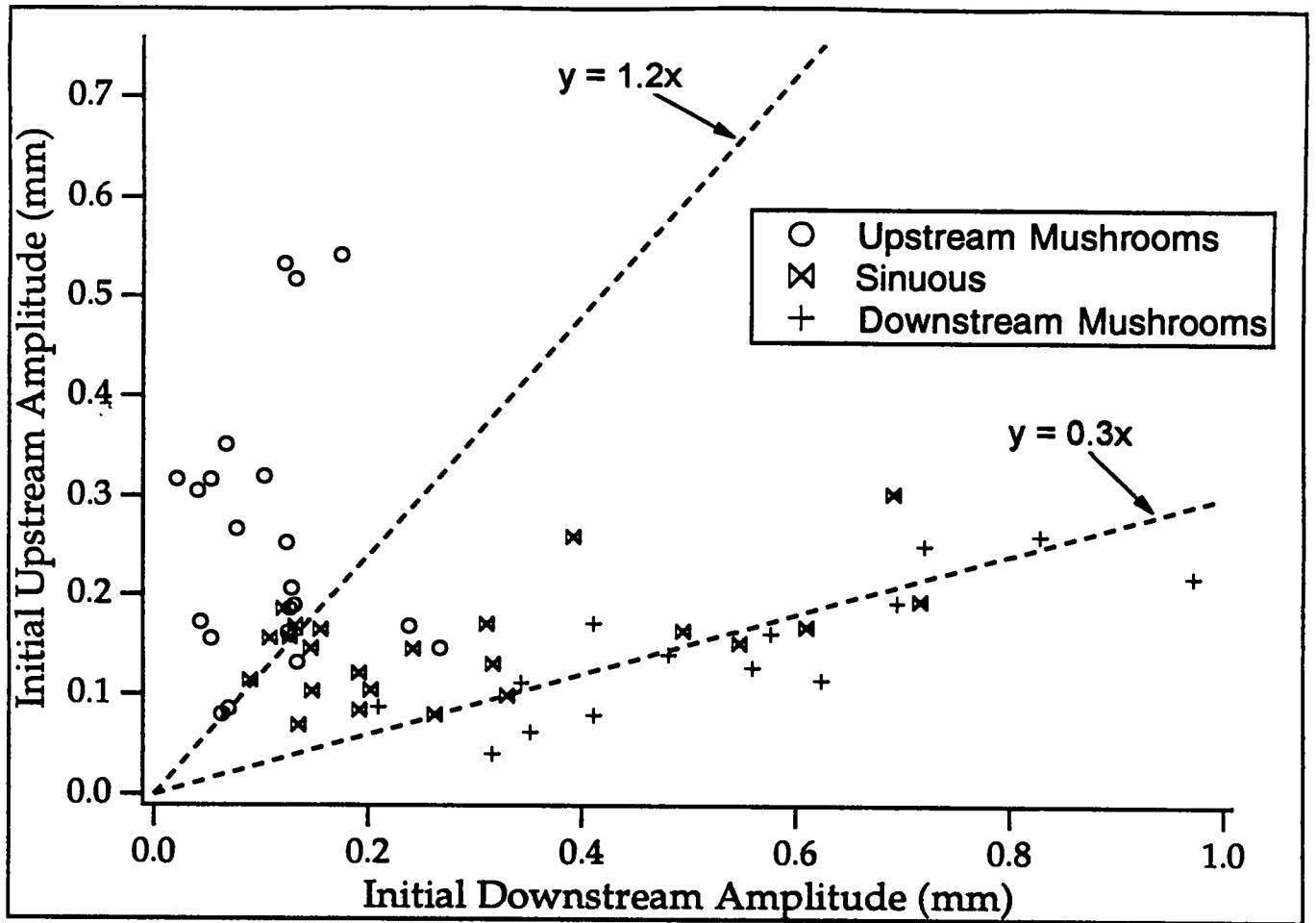


Figure 6. Upstream vs. downstream perturbation amplitudes.

UPCOMING CNLS COLLOQUIA

- Wed., Feb. 1 "Neural Net Representations of Empirical Protein Potentials," Tal Grossman, CNLS/T-13, 3:00 p.m., CNLS Conference Room, followed by tea and cookies
- Fri., Feb. 3 "Operability and Stability of Viscous Free Surface Flows," Kostas N. Christodoulou, DuPont Central Research and Development, 10:30 a.m., CNLS Conference Room
- Tues., Feb. 7 "Failure of Fiber Composites: A Lattice Green's Function Model," S. J. Zhou, CNLT/T-11/T-12, 10:30 a.m., CNLS Conference Room, **CNLS Materials Seminar Series**
- Wed., Feb. 8 "A New Numerical Simulation Algorithm for Stochastic Differential Equations," Tim Elston, CNLS, 3:00 p.m., CNLS Conference Room, followed by tea
- Fri., Feb. 10 "Atomistic Study of Cleavage and Dislocation Emission in NiAl," Peter Gumbsch, Max-Planck Inst., 10:00 a.m., CNLS Conference Room, **Joint CNLS/T-12/T-11 Seminar**
- Mon., Feb. 13 "The Gibbs Phenomenon and Its Role in Scientific Computing." David Gottlieb, Brown Univ., 10:00 a.m., CNLS Conference Room, **CNLS/UNM Distinguished Lecture**
- Mon., Feb. 13 "High Order Difference Schemes in Shock Waves," David Gottlieb, Brown Univ., 1:30 p.m., CNLS Conference Room, **CNLS/UNM Distinguished Lecture**
- Mon., Feb. 13 "Why Call It HARD Turbulence When It's So Easy?" Joe Werne, NCAR, 3:30 p.m., CNLS Conference Room
- Tues., Feb. 14 "Guiding the Synthesis of Catalytic Materials with Theory and Simulation," Tony Redondo, T-12, 10:30 a.m., CNLS Conference Room, **CNLS Materials Seminar Series**
- Thurs, Feb. 16 "Bénard Convection: New Experimental Results," Mike Schatz, Univ. of Texas, Austin, 10:30 a.m., CNLS Conference Room
- Thurs, Feb. 16 "Spatio-Temporal Patterns in Silent Discharges," Beth Gwinn, Univ. of California, Santa Barbara, 1:00 p.m., CNLS Conference Room
- Fri., Feb. 17 "Resonances in Driven Dynamical Lattices," Boris Malomed, Tel-Aviv Univ., 9:30 a.m. CNLS Conference Room
- Fri., Feb. 17 "Stability by Enstrophy Dissipation for Two-Dimensional Shear Flow," Isom Herron, Rensselaer Polytechnic Inst., 1:30 p.m., CNLS Conference Room

CNLS PUBLICATIONS - NEW RELEASES

- 95-0017 C. Elphick, A. Hagberg and E. Meron, "Dynamic Front Transitions and Spiral-Vortex Nucleation"
- 95-0064 S. Zhang, J. Carlson and J. E. Gubernatis, "A Constrained Path Quantum Monte Carlo Method for Fermion Ground States"
- 95-0065 J. Riordan, C. R. Doering and D. Ben-Avraham, "Fluctuations and Stability of Fisher Waves"
- 95-0070 W. Choi, "Nonlinear Evolution Equations for Two-Dimensional Surface Waves in a Fluid of Finite Depth"
- 95-0181 L. G. Reyna and J. R. Sobehart "The Repetition Rate Effect on the Ablation by UV-Lasers of Polymer Structures"

INTRODUCTION TO LONG-TERM VISITORS, STUDENTS AND POSTDOCS

Our most recent arrivals and very brief interests:

Anil Bangia, Princeton Univ., pattern formation in reaction-diffusion and fluid flow

Mark Johnson, Princeton Univ., simulation methods for advanced scientific computing

David Ropp, Univ. of Arizona, nonlinear waves

UPCOMING CNLS WORKSHOPS

Title	Dates	Location	Technical Host
Colorado Days	3/17-18	Boulder, CO	N. Tuffiaro
Fractal Analysis and Modeling of Materials	4/26-28	CNLS	R. Blumenfeld A. R. Bishop
Annual 15: Nonlinear Phenomena in Ocean Dynamics	5/15-19	Los Alamos	D. Holm L. Margolin R. Malone R. Smith
Complex Systems Summer School	June	Santa Fe	E. Jen
Mathematical Problems in Industry Workshop	6/12-16	Albuquerque	P. Hagan
Maximum Entropy and Bayesian Methods	7/30-8/4	Santa Fe	R. Silver K. Hanson
Turbulence Theory	August	CNLS	S. Y. Chen G. Doolen L. Margolin B. Nichols

ORGANIZATION OF THE CENTER

Charlie Doering, 7-1444
Susan Coghlan, 5-1556
Frankie Gomez, 7-1444
Dorothy Garcia, 7-1444
Lisa Gardner, 7-1444
Janet Pacheco-Morton, 7-1444
Barbara Rhodes, 7-1444
Rose Vigil, 7-1444

Deputy Director
Systems Manager
Staff Assistant
Secretary
Secretary
Secretary
Secretary
Secretary

For more information on newsletter items or for suggestions for future issues, contact Barbara Rhodes, (505) 667-1444, MS-B258, by FAX at (505) 665-2659, or by e-mail at "office@cns.lanl.gov"

Los Alamos National Laboratory, an Affirmative Action/Equal Opportunity Employer, is operated by the University of California for the United States Department of Energy under contract W-7405-ENG-36.

LOS ANGELES NAT'L LAB.
LIB. REPT. COLLECTION
RECEIVED

'95 FEB 6 AM 2 30